

An Integrated ANN–GA-Based Framework for Multi-Parameter Design Optimization of a Large-Scale 3D Concrete Printer Frame in a Discrete Design Space

Duc Hai Ta – Dinh Tung Pham – Van Binh Phung ✉
Le Quy Don Technical University, Hanoi, Vietnam
✉ phungvanbinh@lqdtu.edu.vn

Abstract *This paper presents an integrated artificial neural network-genetic algorithm (ANN-GA)-based framework for multi-parameter design optimization of a large-scale concrete 3-dimensional (3D) printer frame in a discrete design space. Based on practical design requirements and operating conditions, a finite element (FE) model of the printer frame is developed using APDL® scripting, enabling automated evaluation of printhead deflection and natural frequencies. Using the FE-generated dataset, a multilayer feed-forward neural network (MLFFNN) is trained as a surrogate model to predict the structural responses of the frame. Parametric investigations demonstrate that the artificial neural network (ANN) surrogate model substantially reduces computational time while maintaining high prediction accuracy, with errors ranging from 1 % to 4 % compared to direct FE analysis. A mass-minimization optimization model is then formulated with ten design variables and four constraints related to printhead deflection and natural frequencies. Genetic algorithms are employed to solve the optimization problem using two different approaches: direct optimization coupled with FE analysis and surrogate-based optimization using the ANN model. Notably, the optimization is conducted in a discrete design domain consistent with the standard dimensions of commercially available steel box sections. The optimal solutions obtained from different optimization strategies, including continuous and discrete FE-based models, the ANN surrogate model, and an experience-based design, are systematically compared. The optimization results demonstrate that the proposed framework achieves a structural weight reduction of 27 % to 38 % compared to the initial experience-based design. Furthermore, the ANN-based surrogate optimization reduces the total computational time from approximately 38 hours to about 200 seconds, clearly demonstrating the efficiency and practical applicability of the proposed approach for real-world large-scale machine design.*

Keywords *3D concrete printer frame, design optimization, ANN surrogate model, integrated ANN-GA approach*

Highlights

- *An integrated ANN-GA framework is proposed for optimizing a large-scale concrete 3D printer frame.*
- *A high-fidelity FE model is automated using ANSYS APDL® to generate training data for surrogate modeling.*
- *Design optimization is performed in both continuous and discrete domains, consistent with practical manufacturing constraints.*
- *The performance of direct FE-based and ANN-based surrogate optimization is compared in terms of accuracy and computational efficiency.*

1 INTRODUCTION

Concrete 3D printing (C3DP) has developed rapidly in recent years as an effective automation solution for the construction industry, enabling the direct fabrication of complex concrete components from digital models [1]. This technology significantly shortens construction time, reduces the need for formwork, and improves material efficiency [2]. At present, C3DP has been widely applied in residential construction, temporary and emergency shelters, as well as free-form architectural components [3]. Large-scale concrete 3D printing systems can generally be classified into three main configurations: robotic arm–based systems, crane- or cable-driven systems, and gantry-type systems. While robotic arm systems offer high flexibility, they are often limited in terms of workspace size and structural stiffness, whereas cable-based systems face challenges in achieving high printing accuracy and operational stability. In contrast, gantry-type configurations are characterized by high structural stiffness, good positioning accuracy, and scalable working envelopes, and they can be deployed for both indoor and outdoor printing applications [4]. Owing to these advantages, gantry-based concrete 3D printers are frequently adopted for large-scale printing applications [5,6], which in turn highlights the necessity of optimizing the gantry frame design to simultaneously satisfy requirements related to structural strength, stiffness, and overall operational performance [7,8].

Among the key components, the mechanical frame structure of a concrete 3D printer plays a critical role, as it directly influences structural stiffness, printing accuracy, and operational speed. However, designing a printer frame that is simultaneously lightweight, durable, and cost-effective remains a significant challenge, particularly under the pressure of shortened product development cycles. At present, most machine frame designs still rely heavily on engineering experience combined with conventional numerical simulation tools, such as finite element analysis (FEA). Two main design optimization approaches are commonly adopted. In the first approach, a factorial design is constructed to determine a limited number of design configurations to be evaluated. FEA is then performed for the selected parameter sets, followed by the development of surrogate models, such as regression model [9], response surface models (RSM) [10], or Kriging surrogate model [11], to approximate performance criteria based on simulation data. Subsequently, optimization is carried out using the established surrogate models. Although this approach is relatively straightforward and requires a limited number of design evaluations, its major drawback lies in the limited accuracy of the surrogate models, which may prevent the obtained solutions from being truly optimal. An alternative approach involves the direct integration of optimization algorithms with FEA software. For instance, Du et al. [12] proposed a design methodology for metro underframe structures based on a topology–size–shape co-

 DOI: 10.5545/sv-jme.2026.1638

optimization framework. In this approach, the optimization process is conducted within commercial FEA software (e.g., OptiStruct), where objective functions and constraints are evaluated using embedded finite element (FE) solvers in conjunction with gradient-based sensitivity analysis. While this strategy ensures high accuracy and strong physical consistency, it relies heavily on repeated high-fidelity simulations, leading to substantial computational cost [13]. Consequently, it becomes inefficient for complex optimization problems characterized by high-dimensional design spaces, multiple constraints, and competing performance objectives.

To reduce computational costs, many researchers have introduced artificial neural networks (ANNs) in mechanical engineering to model and predict the structural behavior of mechanical systems. ANNs have been demonstrated to be effective surrogate modeling techniques for approximating complex nonlinear relationships between design parameters and structural responses, particularly with respect to mechanical deformation, stress distribution, and modal characteristics. Numerous studies have successfully applied ANN-based models to a wide range of structural engineering problems. For example, Tran et al. proposed a practical ANN-based approach for estimating the punching shear strength of two-way reinforced concrete slabs [14]. Vu et al. [15] employed ANN models to predict the ultimate axial compressive capacity of concentrically loaded concrete-filled double-skin steel tube columns. In the context of stability and dynamic analysis, Papazafeiropoulos et al. [16] utilized deep learning techniques to determine buckling coefficients of stiffened plate girders under pure bending, and Wu et al. [17] developed a deep convolutional neural network to estimate structural dynamic responses. In addition, ANN-based and machine learning approaches have been applied to the modeling of composite structures, such as soft fiber-reinforced bending actuators [18], concrete-filled rectangular steel tube columns [19], and adhesively bonded joints with viscoelastic layers [20].

Building upon their strong predictive capability, ANN models have also been widely employed as surrogate models in design optimization problems. This approach effectively addresses two critical challenges: improving model accuracy while significantly reducing computational cost. By replacing repeated high-fidelity numerical simulations with accurate surrogate models, ANN-based optimization frameworks enable efficient exploration of complex design spaces while maintaining acceptable prediction accuracy. Consequently, the integration of ANN with metaheuristic optimization algorithms has gained increasing attention in recent years. Several studies have reported successful applications of hybrid ANN-based optimization frameworks. Jiang and Gao [21] proposed an optimization program for rail profile design based on a coupled ANN-genetic algorithm (GA) approach. Liu et al. [22] performed minimum-weight optimization of laminated composite structures using ANN-GA surrogate models. Zhang [23] presented an integrated ANN-particle swarm optimization (PSO)–FEM framework for the optimal design of planar irregular reinforced concrete structures, while Liu et al. [24] developed a hybrid GA for truss optimization based on deep neural networks. In addition, ANN-assisted optimization approaches have been successfully applied to practical mechanical systems, including composite running blade prosthetics [25] and rubber engine mounts [26].

Despite these advances, the application of ANN beyond predictive modelling, specifically for the design and optimization of complex real-world mechanical structures, remains relatively limited. Most existing studies focus either on purely predictive modelling [13-20] or on the optimization of structural components with design parameters defined in a continuous domain [21-26]. As a result, the optimized dimensional parameters may not comply with actual manufacturing constraints and must be rounded to the nearest available standard sizes. This adjustment reduces the effectiveness of the optimization results. A review of the literature reveals that the integration of ANN with optimization algorithms, such as GA or PSO, to form a surrogate-based optimization loop is still an emerging area, particularly in the design of large-scale machinery such as 3D concrete printers, large Computer Numerical Control (CNC) machines, or construction robots. These systems involve multiparameter with nonlinear constraints, making them ideal candidates for intelligent optimization approaches, yet real-world applications remain scarce. This gap presents an opportunity to advance the field by developing hybrid ANN-optimization frameworks tailored for the design of specific machine structures. Such frameworks could enable efficient exploration of large design spaces with reduced computational costs, while still accounting for the physical fidelity of real systems.

To address this gap, the present study proposes an integrated ANN-GA approach for optimizing the frame structure of a large-scale concrete 3D printer, representing a real-world complex mechanical system with multiple design parameters and constraints. A surrogate model based on ANN is constructed using simulation data generated from FEA via Ansys parametric design language (APDL) scripting, and a GA is employed to perform the optimization under multiple structural constraints. The proposed framework also considers design variables in a discrete domain consistent with standard steel sections, enabling practical manufacturability. The effectiveness of the proposed approach is evaluated through a systematic comparison with alternative optimization strategies.

The main contributions of this study can be summarized as follows:

1. A discrete design space formulation aligned with standard steel sections, ensuring direct manufacturability of optimized solutions;
2. Application to a real large-scale gantry-type 3D concrete printer frame with coupled static and dynamic constraints;
3. Development of an integrated dual optimization framework combining direct FE-based and ANN-based surrogate approaches, with systematic comparison and verification;
4. A clear quantitative demonstration of computational efficiency, showing a reduction in optimization time from approximately 38.5 hours to about 200 seconds while maintaining acceptable accuracy.

The remainder of this paper is organized as follows. Section 2 presents the materials and methods employed in this study. Section 3 presents the results and discussion. Finally, Section 4 summarizes the main conclusions of the study.

2 MATERIALS AND METHODS

2.1 Large-scale 3D Concrete Printer Frame

The printer frame is designed based on a space frame structure system [27]. A preliminary design of the printer is illustrated in Fig. 1. The Y-axis and Z-axis frames are assembled from steel box beams with standard square cross-sectional dimensions. The printer legs consist of a sliding rail system, with the rails directly fixed to the construction foundation and fabricated from I-beam steel structures.

Some fundamental technical requirements of the large-scale 3D concrete printer are defined as follows [27]:

- Maximum printable structure dimensions: 6000 mm × 4000 mm × 3500 mm.
- Printhead travel speed V ranging from 0 m/min to 20 m/min.
- Permissible positioning error of the printhead: ±5 mm in the X and Y directions, and ±2 mm in the Z direction.

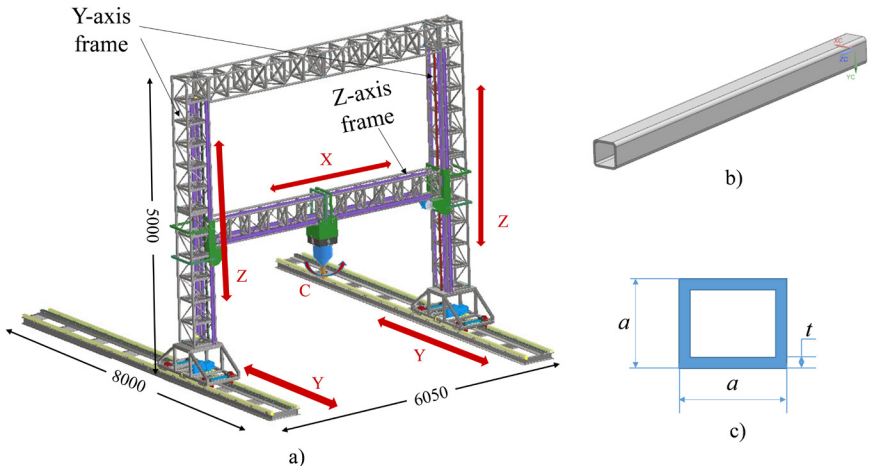

Fig. 1. An experience-based design of a large-scale 3D concrete printer; a) 3D model of the printer; b) 3D model of the steel box beam; and c) cross-sectional view of the box beam

2.2 Structural Modeling

2.2.1 Governing Equations

The printer frame is analyzed using the finite element method (FEM). The static equilibrium equations for the structure are described by Eq. (1). From these, the nodal displacements u are calculated by solving the system of static equilibrium equations [28], as shown in Eq. (2):

$$\mathbf{Ku} = \mathbf{F}, \tag{1}$$

$$\mathbf{u} = \mathbf{K}^{-1}\mathbf{F}, \tag{2}$$

where $\mathbf{K}$ is the global element stiffness matrix, $\mathbf{u}$ is nodal displacement vector, and $\mathbf{F}$ is the external force vector.

The natural mode shapes and frequencies of the printer frame during free vibration are determined through modal analysis [29], based on Eq. (3):

$$\mathbf{M\ddot{u}} + \mathbf{Ku} = 0, \tag{3}$$

where, $\mathbf{M}$ is mass matrix, and $\ddot{\mathbf{u}} = d^2\mathbf{u}/dt^2$ is the 2nd time derivative of the nodal displacement vector $\mathbf{u}$.

To solve Eq. (3), it is assumed that the system undergoes harmonic vibration with a solution of the form Eq. (4):

$$\mathbf{u}(t) = \boldsymbol{\phi}\sin(\omega t + \theta). \tag{4}$$

Substituting this expression into the equation of motion yields an eigenvalue or characteristic value problem, as expressed in Eq. (5):

$$\left(\mathbf{K} - \omega^2\mathbf{M}\right)\boldsymbol{\phi} = 0, \tag{5}$$

where, ω is the natural angular frequency and $\boldsymbol{\phi}$ represents vector of the shape of the system (mode shape). Solving Eq. (5) allows the determination of the values of ω_i (from which the natural frequencies $f_i = \omega_i/(2\pi)$ can be derived) and their corresponding mode shapes ϕ_i.

In this study, the global stiffness matrix $\mathbf{K}$ and mass matrix $\mathbf{M}$ are constructed from the finite element model of the printer frame (see the FE model description). The geometric design parameters of the frame, including $c_X, c_Y, a_1, t_1, a_2, t_2, a_3, t_3, a_4, t_4$ (Fig. 2), directly influence the stiffness matrix $\mathbf{K}$, thereby governing the nodal displacements $\mathbf{u}$ and, in particular, the printhead displacement, as defined in Eq. (2).

These design parameters also determine the mass matrix $\mathbf{M}$, which subsequently governs the natural frequencies f_i of the structure through the eigenvalue problem given in Eq. (5).

2.2.2 FE Model

The FE model of the printer frame was developed using Ansys APDL® software. The parameters of the preliminary design configuration are presented in Table 1. A total of ten dimensional parameters were parameterized to enable automated calculations across different sets of parameters. In particular, c_X and c_Y represent the width of the Y-axis frame in the X and Y directions, respectively; $a_1 \times a_1 \times t_1$ denotes the cross-sectional dimensions (vertical × horizontal × thickness) of the square steel box beam in the Y-axis frame; $a_2 \times a_2 \times t_2$ denotes the cross-sectional dimensions of the square steel box beam in the Z-axis frame; $a_3 \times a_3 \times t_3$ denotes the cross-sectional dimensions of the diagonal reinforcement members used in both the Y-axis and Z-axis frames; $a_4 \times a_4 \times t_4$ denotes the cross-sectional dimensions of the steel box beam at the base of the Y-axis frame.

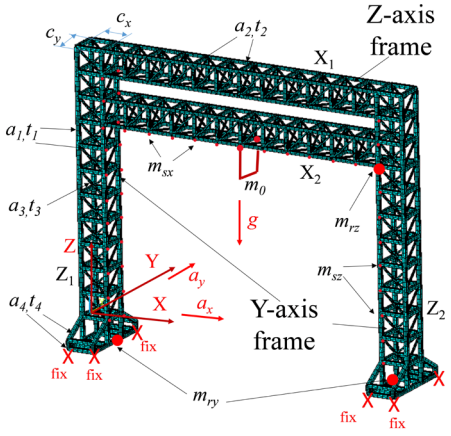

Fig. 2. FE model of printer frame

Table 1. The experience-based design parameters of the printer frame [mm]

c_X	c_Y	$a_1 \times a_1 \times t_1$	$a_2 \times a_2 \times t_2$	$a_3 \times a_3 \times t_3$	$a_4 \times a_4 \times t_4$
460	460	60×60×3	50×50×2.5	25×25×1	60×60×3

The design problem is inherently discrete because the key parameters are selected from a finite set of commercially available profiles and standard manufacturing dimensions. Table 2 provides a detailed description of the feasible value sets for parameters c_X, c_Y, as well as a_i and t_i.

The steel box beams of the printer frame are modeled using BEAM188 elements. The mass of the print head and the X-axis motor is $m_0 = m_{di} + m_{rx} = 250$ kg, and is represented by a concentrated mass element (MASS21). The total mass of the driving and guiding rails attached to the Y-axis frame is $m_{sy} = 140$ kg, which is assumed to be evenly distributed among the nodes of the Y-axis frame. The total

mass of the driving and guiding rails attached to the Z-axis frame is m_{sz}=100 kg, and is similarly distributed among the nodes of the Z-axis frame. The mass of each Y-axis motor is m_{ry}=25 kg, while the mass of each Z-axis motor is m_{rz}=15 kg. These motors are modeled using concentrated mass elements (MASS21).

To simplify the analysis, the printer frame is assumed to be stationary (the base is fully fixed), and the dynamic loads acting on the frame during motion are converted into equivalent inertial forces. These inertial forces are calculated based on the maximum acceleration experienced during operation. According to the design requirements, the maximum horizontal speed of the print head is V_{max}=20 m/min=0.333 m/s. Assuming the print head reaches this velocity within Δt=0.1 s, the maximum acceleration is estimated to be a_{max}=3.33 m/s² (in the X and Y directions).

Table 2. Parameter description of the frame of a large-scale 3D concrete printer

Geometry parameters	The design parameter set [m]
c_x, c_y	{0.30, 0.32, 0.34, …, 0.54, 0.56, 0.58, 0.60}
a_1, a_2, a_3, a_4	{0.03, 0.038, 0.04, 0.05, 0.06, 0.075}
t_1, t_2, t_3, t_4	{0.001, 0.0011, 0.0012, 0.0014, 0.0016, 0.0018, 0.002, 0.0025, 0.0028, 0.003, 0.0032, 0.0035}

The configuration of the frame under investigation corresponds to the structural state that may cause the greatest positioning error of the print head (i.e., when the Z-axis frame is at its highest vertical position and the print head is located at the center of the Z-axis frame, which may result in the largest deflection).

To reduce computation time, automatic analysis modules were developed using Ansys APDL scripting language, including modules for calculating the displacements of the print head in the X, Y, and Z directions, as well as the natural frequencies of the system [27]. These structural characteristics can therefore be evaluated automatically.

2.3 ANN Model Development

To construct the dataset, a total of 5000 samples were generated using the Ansys APDL-based FE model. Each sample corresponds to a unique combination of input design variables selected within their predefined bounds. The design points were generated using a Monte Carlo-based sampling strategy over the design space. This approach ensures a broad and representative coverage of the design domain while avoiding the combinatorial explosion associated with full factorial sampling.

The dataset generation process was implemented through an automated MATLAB–Ansys APDL script using an iterative loop, where each design variable was discretized within its lower and upper bounds. At each iteration, a set of input parameters was randomly sampled from the corresponding discrete value sets, and the associated structural responses were evaluated using the FE model. This procedure enables efficient exploration of the discrete design space while maintaining a manageable dataset size.

The complete dataset was randomly divided into three subsets, including 70 % for training, 15 % for validation, and 15 % for testing. The training set was used to update the network weights, the validation set was employed to monitor the training process and prevent overfitting, and the test set was used to evaluate the generalization capability of the trained model.

Prior to training, all input and output data were normalized using min–max scaling to eliminate discrepancies in magnitude and ensure stable convergence. Based on the normalized dataset, an ANN surrogate model was developed to efficiently approximate the structural responses required for optimization. Multilayer feed-forward neural networks (MLFFNNs) are widely used in nonlinear regression, classification, and system modeling due to their universal approximation capability [30,31]. In this section, the authors employ a MLFFNN to approximate the response of a 3D printer frame structure, including displacement values (u_X, u_Y, u_Z) and natural frequency (f_1), as a substitute for the Ansys APDL computation module described in Section 2.2. The network consists of an input layer with 10 parameter variables $c_X, c_Y, a_1, a_2, a_3, a_4, t_1, t_2, t_3, t_4$, two hidden layers, and output layer, where information flows unidirectionally from input to output without forming cycles. Each layer performs an affine transformation followed by a nonlinear activation function, enabling the network to learn complex nonlinear mappings between inputs and outputs.

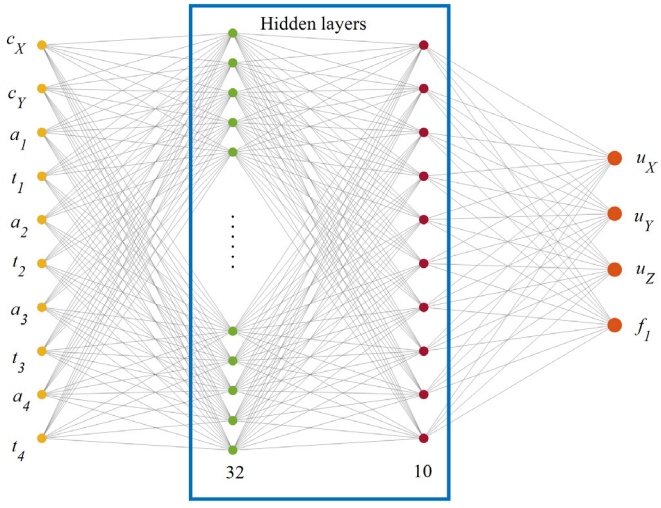

Fig. 3. Architecture of the multilayer feed-forward neural network (MLFFNN)

The MLFFNN was initialized, and its architecture is illustrated in Fig. 3. There are some transfer functions that could be applied, such as log-sigmoid transfer function (*logsig*), linear transfer function (*purelin*), hyperbolic tangent sigmoid transfer function (*tansig*), and hard limit transfer function (*hardlim*). In this study, the hyperbolic tangent sigmoid function was employed as the activation function for the two hidden layers, while a linear function was used in the output layer. The *tansig* function was selected due to its strong capability in capturing complex nonlinear relationships and its output range of [−1 1], which is well suited for normalized input data and contributes to stable and efficient training. In contrast, the linear activation function in the output layer is appropriate for modeling continuous target variables, such as displacement components and natural frequency, enabling the network to produce unbounded outputs and improving regression accuracy [9,32].

The optimal number of neurons in the hidden layers was determined through a systematic trial-and-error procedure based on the evaluation of the mean squared error (MSE) on the validation dataset. The number of neurons was gradually varied within a reasonable range to balance model accuracy and generalization capability, while avoiding overfitting. Based on this analysis, the network architecture with 32 neurons in the first hidden layer and 10 neurons in the second hidden layer was selected.

2.4 Optimization Framework

2.4.1 Optimization problem formulation

The design space consists of 10 discrete design variables corresponding to commercially available structural profiles and standard geometric dimensions. To enable efficient genetic operations while preserving the discrete nature of the problem, each design

variable is represented by an integer index mapped to a predefined discrete set. Specifically, for the i^{th} design variable, an integer gene $g_i \in \{1,2,...,m_i\}$ is assigned, where m_i denotes the number of admissible discrete options, and the actual design value is obtained through an inverse mapping function $x_i = f^{-1}(g_i)$. Consequently, the optimization is performed in a 10-dimensional integer-coded search space, while the physical design remains strictly discrete. For each individual, the decoded design variables are used to construct the structural model, from which the maximum displacement, and the first natural frequency are evaluated by the computational Ansys-APDL model (or surrogate ANN model).

The optimization objective is to minimize the total mass of the mechanical frame of the 3D concrete printer, denoted as M in Eq. (6):

$$M = \rho\left[\sum_{i=1}^{m} 4t_1(a_1 - t_1)L_i + \sum_{j=1}^{n} 4t_2(a_2 - t_2)L_j + \sum_{k=1}^{p} 4t_3(a_3 - t_3)L_k + \sum_{l=1}^{q} 4t_4(a_4 - t_4)L_l\right] \rightarrow \min, \quad (6)$$

where ρ is the material density of the steel frame; m, n, p and q represent the number of structural members corresponding to different cross-section types; and L_i, L_j, L_k, L_l denote the lengths of members with cross-sections $a_1 \times a_1 \times t_1$, $a_2 \times a_2 \times t_2$, $a_3 \times a_3 \times t_3$ and $a_4 \times a_4 \times t_4$, respectively.

The constraints require that the displacements in the X, Y, and Z directions (u_X, u_Y, u_Z) remain below specified allowable limits, while the first natural frequency (f_1) must exceed a prescribed minimum value, as defined in Eq. (7):

$$\begin{cases} u_X = \left|g_X\left(c_X, c_Y, a_1, t_1, a_2, t_2, a_3, t_3, a_4, t_4\right)\right| \le 2\,(\text{mm}); \\ u_Y = \left|g_Y\left(c_X, c_Y, a_1, t_1, a_2, t_2, a_3, t_3, a_4, t_4\right)\right| \le 2\,(\text{mm}); \\ u_Z = \left|g_Z\left(c_X, c_Y, a_1, t_1, a_2, t_2, a_3, t_3, a_4, t_4\right)\right| \le 1\,(\text{mm}); \\ f_1 = g_f\left(c_X, c_Y, a_1, t_1, a_2, t_2, a_3, t_3, a_4, t_4\right) \ge 6\,(\text{Hz}); \end{cases} \quad (7)$$

where $c_x, c_y, a_1, t_1, a_2, t_2, a_3, t_3, a_4, t_4$ denote the geometric design parameters of the printer frame, as defined in Section 2.2 and illustrated in Fig. 2.

Constraint handling is implemented using an absolute penalty function approach, whereby violations of the displacement and natural frequency constraints are explicitly incorporated into the fitness function. Standard genetic operators, including selection, integer-based crossover, and mutation, are applied, with all offspring genes confined to their admissible index bounds. An elitism strategy is adopted to retain the best solutions across generations. This discrete index-mapping GA framework enables robust exploration of the combinatorial design space while ensuring that all candidate solutions correspond to manufacturable and structurally feasible configurations.

2.4.2 GA-Based Optimization Framework

A GA-based optimization framework was subsequently established to identify optimal design solutions under multiple constraints. In the domain of optimization, nature-inspired algorithms are frequently adopted owing to their versatility and robust performance across diverse problem classes. These algorithms can be broadly categorized into bio-inspired and physico-chemical-inspired approaches. Representative bio-inspired algorithms include the Cuckoo Search algorithm, the particle swarm optimization (PSO) algorithm [23], and the GA [33], among others. Physico-chemical-inspired algorithms encompass methods such as the harmony search algorithm and the simulated annealing (SA) algorithm [34]. In the present study, a discrete genetic algorithm (DGA) is adopted to minimize the total structural mass of a large-scale 3D concrete printer frame while satisfying both static and dynamic performance constraints. The DGA is selected due to its proven capability in handling discrete, combinatorial, and constrained optimization problems.

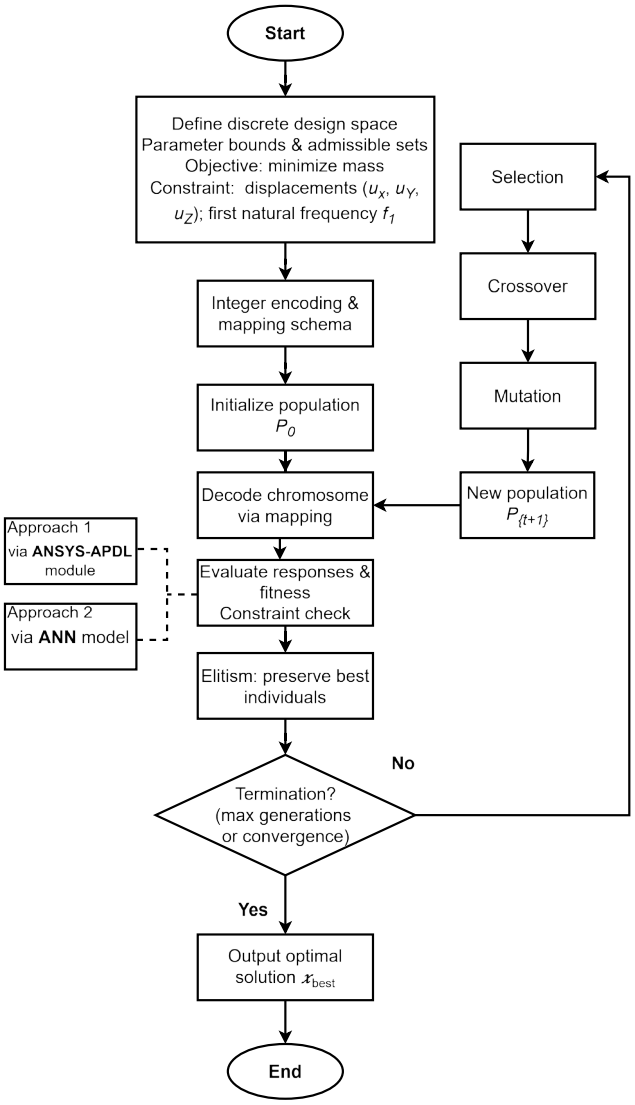

Fig. 4. Flowchart of the GA-based discrete optimization procedure for the 3D printer frame design

Two optimization approaches are considered for the structural design of the large-scale 3D concrete printer frame. The optimization is performed in both continuous and discrete design domains, with the discrete formulation ensuring direct manufacturability using commercially available steel sections.

The first approach follows a conventional finite element-based optimization strategy, in which the DGA is directly coupled with the computational model developed in Ansys APDL (Section 2.2). In this framework, the DGA iteratively updates the design variables, while each candidate solution is evaluated through finite element simulations. The structural responses obtained from the FE model are subsequently used to assess the objective function and design constraints, enabling the search for the optimal frame configuration.

The second approach employs a surrogate-based optimization strategy, in which the computationally expensive Ansys APDL model is replaced by the validated ANN surrogate model developed in Section 2.3. The ANN provides rapid predictions of structural responses, including printhead displacements and the first natural frequency, with high accuracy. Consequently, candidate solutions

generated by the DGA can be evaluated efficiently without repeatedly performing FE simulations. The DGA then iteratively updates the design variables based on the ANN predictions to identify the optimal design. This approach significantly reduces computational cost while maintaining satisfactory optimization accuracy.

The optimization procedure based on the DGA is illustrated in Fig. 4. The process begins with the definition of the discrete design space, where 10 geometric parameters of the printer frame are encoded as integer indices within their feasible ranges. Next, the fitness of each individual is assessed according to its structural performance. The elitism strategy is applied to preserve the best-performing individuals, ensuring that superior solutions are carried over to the next generation. The selection operator (e.g., roulette wheel or tournament method) identifies parent chromosomes, which are then combined through crossover and slightly modified through mutation to produce a new population of candidate designs. This iterative evolutionary cycle - evaluation, selection, crossover, and mutation - continues until a termination criterion is met, such as reaching the maximum number of generations or achieving convergence of the objective function. The final output is the optimal design parameter set, representing the best balance between minimum structural displacement and sufficient stiffness, while satisfying the predefined constraint on natural frequency.

3 RESULTS AND DISCUSSION

3.1 Validation of the ANN Surrogate Model

ANN performance evaluation

Figure 5 presents the performance evaluation of the developed ANN model across the training, validation, and testing datasets. The regression plots indicate a very strong correlation between the predicted and target values, with correlation coefficients (R) exceeding 0.9997 for all subsets. This demonstrates the high predictive capability of the proposed model.

The distribution of prediction errors, as illustrated by the error histograms (Fig. 5c), shows that most errors are concentrated around zero with a relatively small dispersion, indicating low bias and good consistency of the model. In addition, the training process exhibits stable convergence behavior, with the MSE reaching a minimum value of 2.20×10^{-5} at epoch 216, suggesting effective learning of the underlying nonlinear relationships.

To quantitatively assess the model performance, several statistical metrics were employed, including the MSE, root mean squared error (RMSE), mean absolute error (MAE) and correlation coefficient R, as summarized in Table 3. These metrics were computed for the independent test dataset to ensure a comprehensive evaluation.

Table 3. Performance evaluation of the ANN model using statistical error metrics for the independent test dataset

Error metric	MSE	RMSE	MAE	R
Independent test dataset	1.053×10^{-4}	1.026×10^{-2}	3.42×10^{-3}	0.9998

3.1.1 Investigation of the Computational Results

In this section, the effects of the input design parameters on the displacement responses and first natural frequency of the print head are investigated. Furthermore, to rigorously validate the predictive capability of the trained ANN, the ANN-based predictions are quantitatively compared with the corresponding results obtained from the high-fidelity Ansys APDL numerical model. This section defines the absolute errors and relative errors between the predictive performance and simulation performance (i.e., Ansys APDL simulated data) to compare the performance of ANN. The calculation formula for absolute error E_{abs} and relative error E_{rel} is:

$$E_{abs} = \left| y_{APDL} - y_{ANN} \right|, \tag{8}$$

$$E_{rel} = E_{abs} / y_{APDL}, \tag{9}$$

where, y_{APDL} is the output response of Ansys APDL module, y_{ANN} is the predicted output of ANN.

The comparison between the predicted displacements obtained from the ANN model and those computed by the finite element analysis in Ansys APDL demonstrates an excellent agreement across all components (u_X, u_Y, u_Z). As shown in Fig. 6a, an increase in the geometric variable c_x leads to a noticeable reduction in u_X and u_Z, indicating an improvement in the global stiffness of the frame along the X-direction. The displacement component u_Y remains nearly constant, implying that the change in c_X has limited influence on lateral stiffness along the Y-axis.

The relative error between ANN predictions and APDL results (Fig. 6b) remains generally below 3 %, with the smallest discrepancies observed in the u_Z component (<1 %). A slight increase in the error of u_X is observed for c_x>450 mm, which may be attributed to nonlinear behavior or sparse sampling in the training dataset within that range. The overall results confirm that the ANN accurately captures the displacement responses.

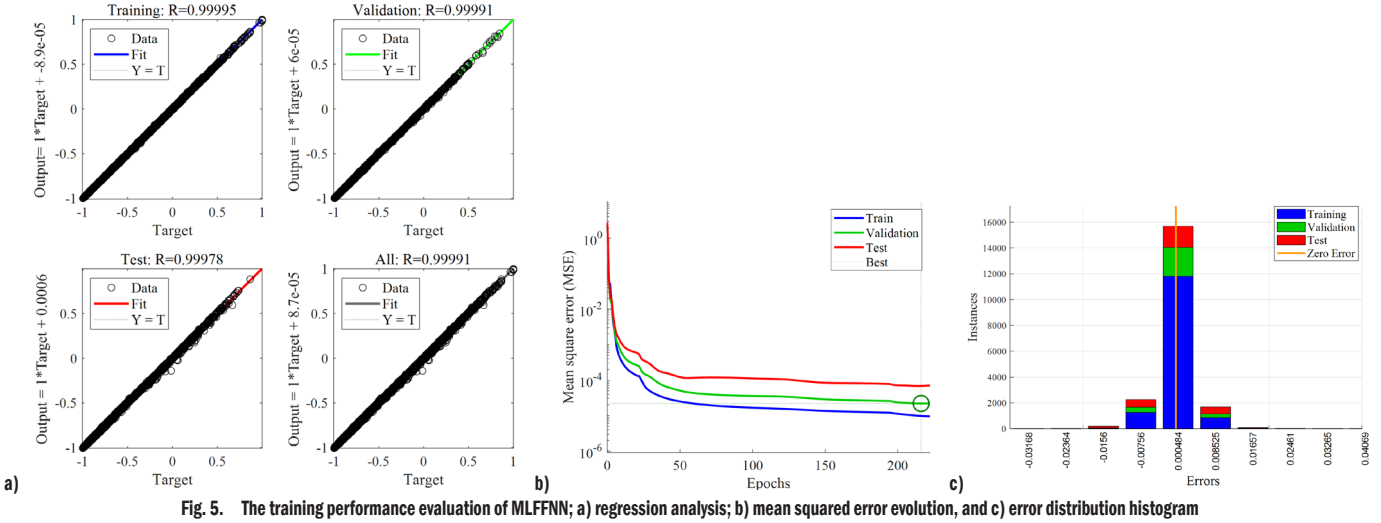

Fig. 5. The training performance evaluation of MLFFNN; a) regression analysis; b) mean squared error evolution, and c) error distribution histogram

Figure 7a presents the variation of the first natural frequency f_1 with respect to c_x. Both ANN and APDL values exhibit similar trends, where f_1 gradually increases as c_x rises, reflecting enhanced global rigidity. The relative error (Fig. 7b) is below 0.6 %, confirming the high accuracy of ANN-based dynamic response prediction.

The influence of parameter c_y is shown in Fig. 8 and 9. The ANN predictions exhibit a strong correlation with APDL results for all displacement components. The dominant variation occurs in u_Y, which decreases markedly with increasing c_Y, signifying enhanced stiffness along the Y-direction. Meanwhile, u_X and u_Z remain nearly stable, as expected for this type of geometric modification.

The relative error between ANN and APDL values remains within 3 %, with a minor increase in u_Y error at higher c_Y values. Such deviation can be explained by the stronger stiffness gradient and nonlinearities at larger dimensions. The corresponding natural frequency f_1 increases monotonically with c_Y, confirming that the structural stiffness is markedly affected by this parameter. The ANN model accurately follows the APDL trend, and the maximum relative error remains below 1.2 %, demonstrating reliable generalization in dynamic analysis.

Figure 10 illustrates the displacement and error distributions corresponding to changes in a_1. With increasing a_1, all displacement components (u_X, u_Y, u_Z) decrease consistently, highlighting an improvement in vertical member stiffness. The ANN model replicates the APDL results with excellent accuracy, exhibiting maximum errors of less than 3 % across all components and below 1 % for u_Z. These findings demonstrate that the ANN effectively captures the parametric relationships governing both the static and dynamic behaviors of the structure.

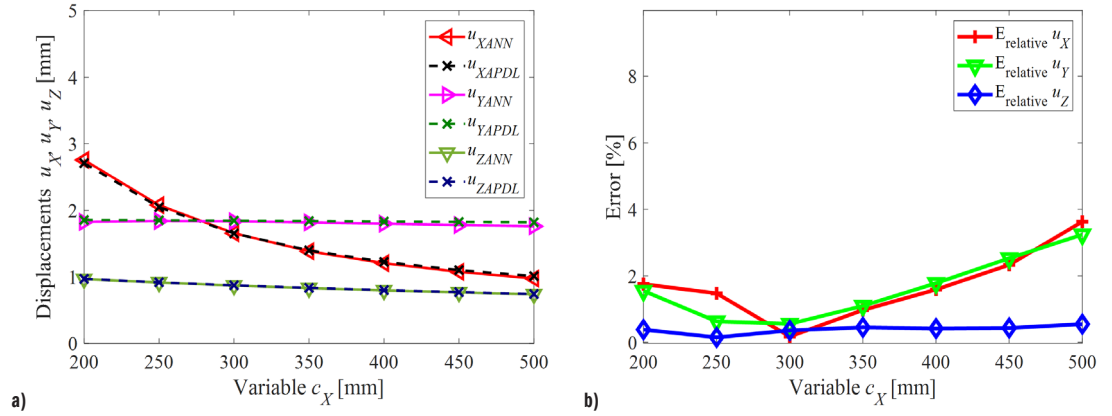

Fig. 6. Comparison of ANN-predicted and Ansys APDL-simulated displacements and their relative errors versus c_X; a) displacement; b) relative error

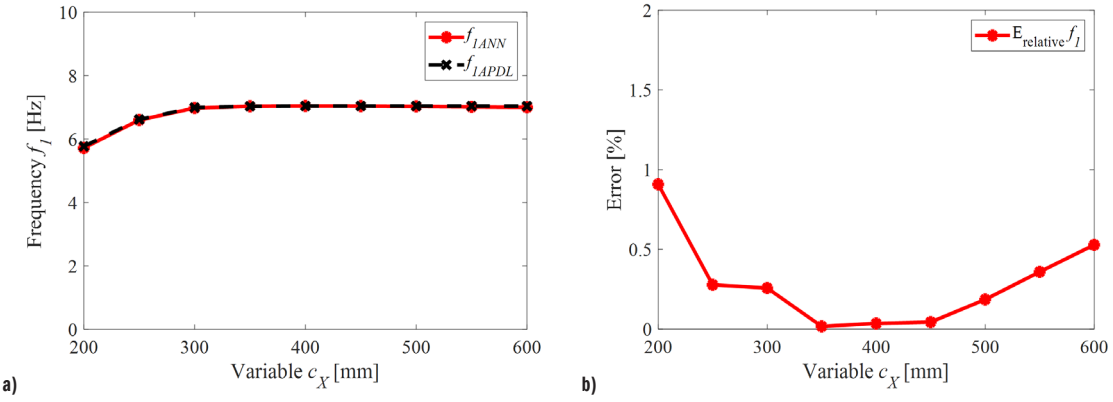

Fig. 7. Comparison of ANN-predicted and Ansys APDL-simulated first natural frequency and the corresponding relative error versus c_X; a) first natural frequency; b) relative error

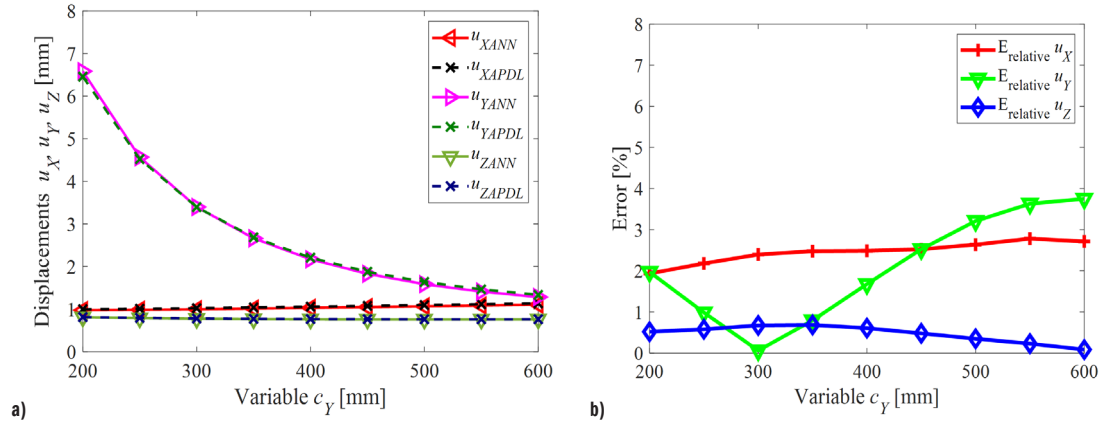

Fig. 8. Comparison of ANN-predicted and Ansys APDL-simulated displacements and their relative errors versus c_Y; a) displacement; b) relative error

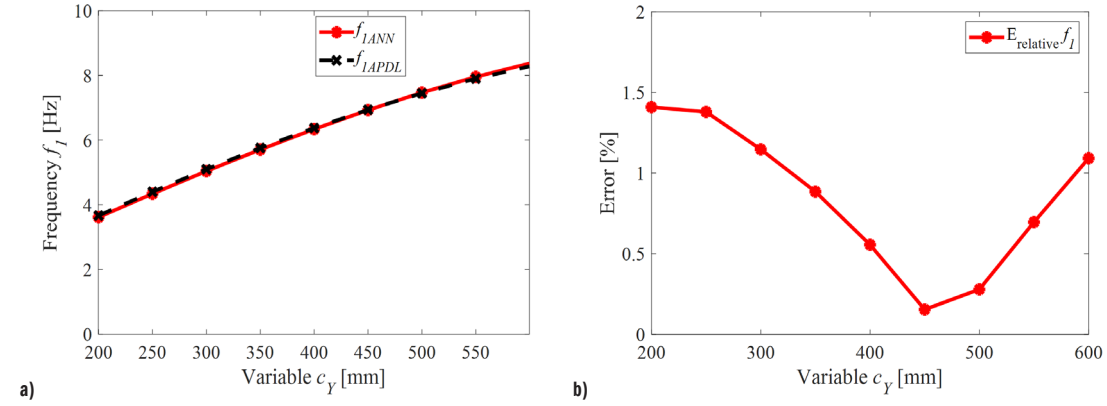

Fig. 9. Comparison of ANN-predicted and Ansys APDL-simulated first natural frequency and the corresponding relative error versus c_Y; a) displacement; b) relative error

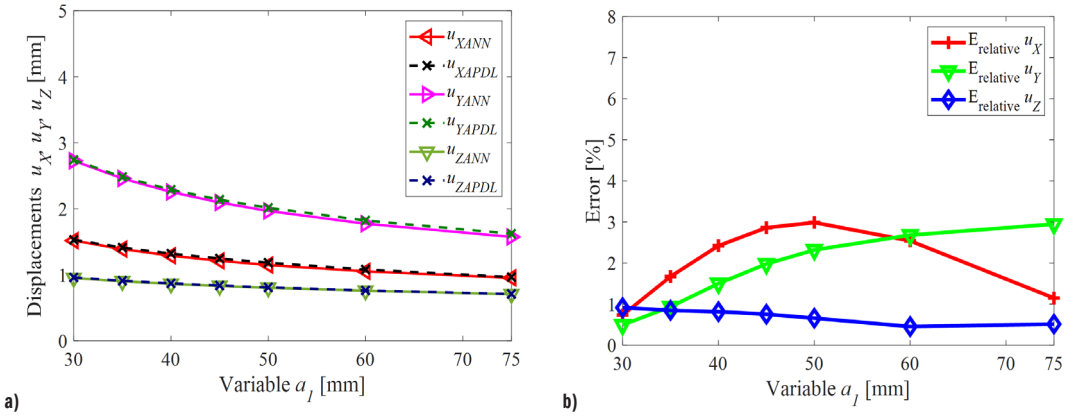

Fig. 10. Comparison of ANN-predicted and Ansys APDL-simulated displacements and their relative errors versus a_1; a) displacement; b) relative error

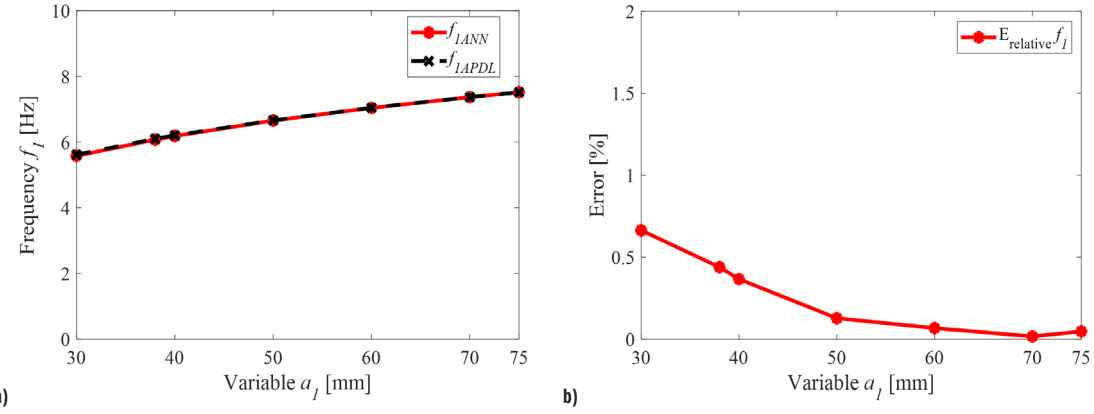

Fig. 11. Comparison of ANN-predicted and Ansys APDL-simulated first natural frequency f_1 and relative errors versus a_1; a) first natural frequency; b) relative error

Figure 11a demonstrates a strong agreement between the ANN-based predictions and the reference APDL results for the first natural frequency f_1 as a function of a_1. The first natural frequency f_1 increases monotonically with a_1, indicating that enlarging a_1 enhances the global stiffness of the frame and consequently raises its fundamental vibration frequency. The ANN curve almost completely overlaps the APDL curve across the investigated range, confirming the high fidelity of the surrogate model in capturing the dynamic trend. The error plot in Fig. 11b further verifies this accuracy. The relative error remains consistently low (below approximately 0.7 %) and decreases as a_1 increases, reaching nearly zero at larger values of a_1. This behavior suggests that the ANN model provides a highly reliable approximation of the APDL-based frequency response, with improved prediction stability in the higher a_1 region.

Figures 12 and 13 illustrate the variation of displacement components, relative errors, and the first natural frequency of the 3D concrete printer frame with respect to the geometric parameter t_1. An increase in the geometric parameter t_1 leads to a gradual reduction in all displacement components (u_X, u_Y, u_Z), indicating improved structural stiffness. Among them, u_Y exhibits the most pronounced decrease, highlighting the strong influence of t_1 on stiffness in the Y-direction. The ANN predictions show excellent agreement with the APDL results over the entire investigated range. The relative errors remain below 3 % for u_X and u_Y, and below 1 % for u_Z, confirming the reliability of the surrogate model. The first natural frequency f_1 increases monotonically with increasing t_1, reflecting enhanced global rigidity of the frame. The ANN accurately reproduces the APDL results, with a maximum relative error of approximately 0.35

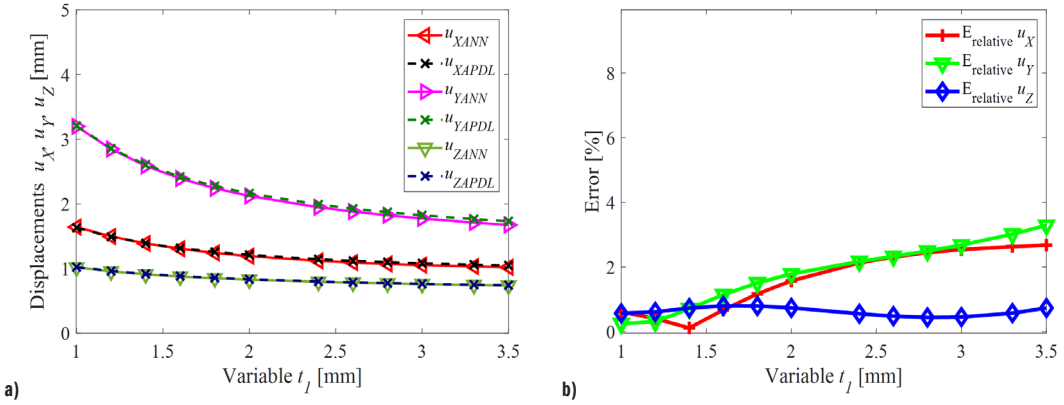

Fig. 12. Comparison of ANN-predicted and APDL-computed displacement components versus parameter t_1; a) displacement; b) relative error

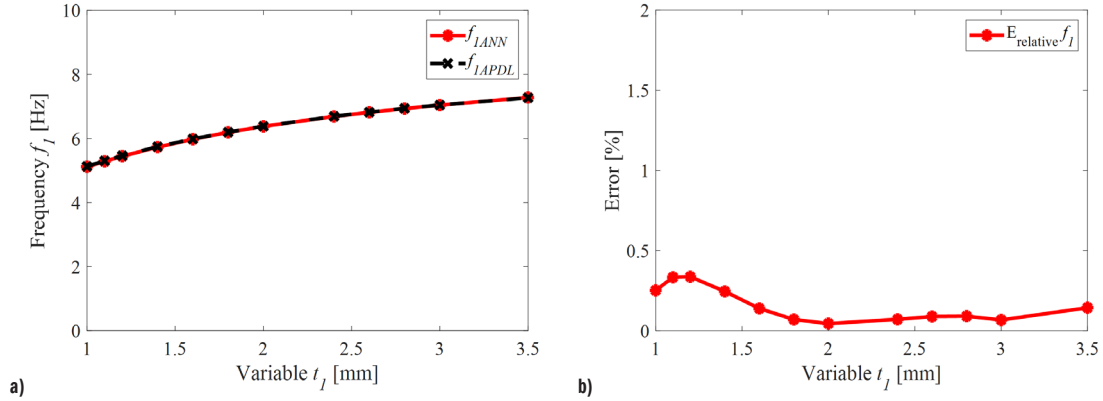

Fig. 13. Comparison of ANN-predicted and Ansys APDL-simulated first natural frequency and the corresponding relative error versus t_1; a) first natural frequency; b) relative error

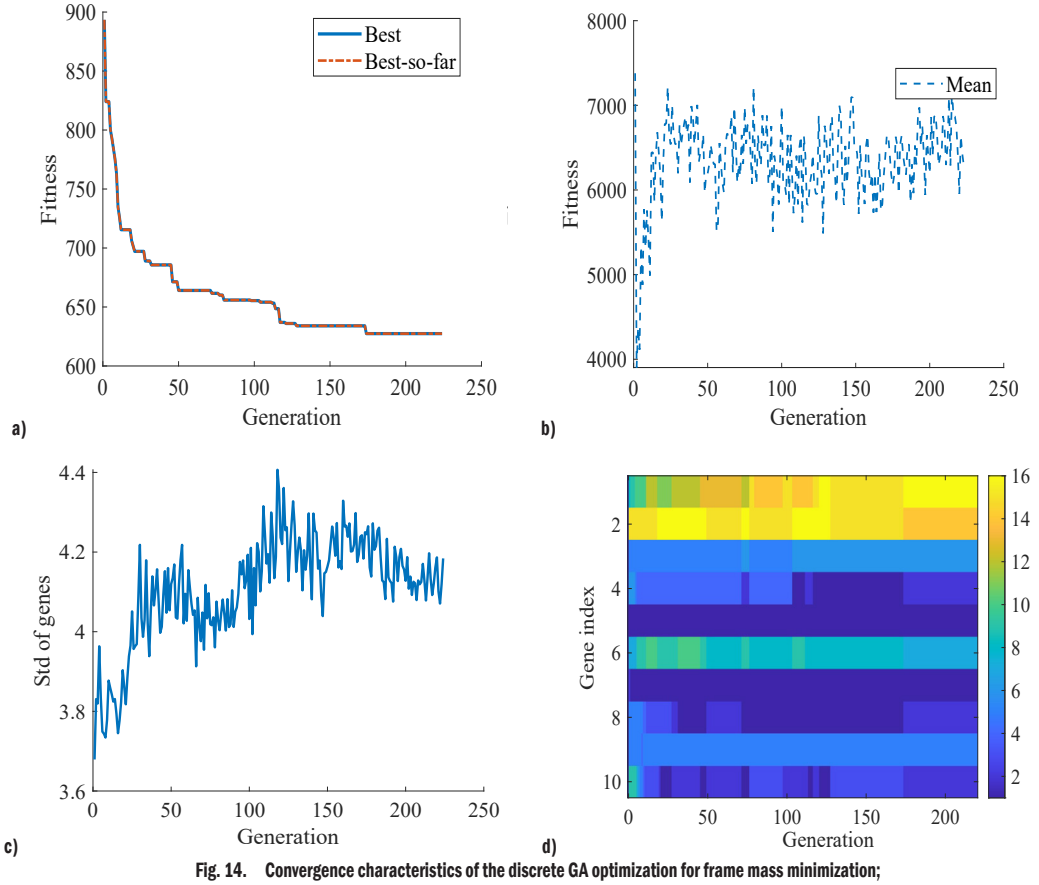

Fig. 14. Convergence characteristics of the discrete GA optimization for frame mass minimization; a) best and best-so-far fitness values, b) mean fitness value, c) population diversity, andd) evolution of the best individual

%. These results demonstrate that the ANN model can efficiently and accurately predict both static and dynamic responses associated with variations in t_1.

Within the limited scope of this paper, the authors do not present a comprehensive investigation of the effects of the remaining input variables on the static and dynamic characteristics. However, the obtained results are highly reliable and exhibit small errors, similar to those observed for the variables c_X, c_Y, a_1, t_1. Overall, the ANN model trained using Matlab–Ansys APDL datasets exhibits high accuracy and stability in predicting both displacement and natural frequency responses of the 3D concrete printer frame. The relative error remains within 4 % for displacements and below 1 % for natural frequency, confirming the model's robustness. These results validate the ANN's ability to serve as a computationally efficient surrogate model, capable of replacing conventional finite element simulations in parametric optimization and design sensitivity analyses of large-scale additive manufacturing systems.

3.2 Optimization Results

3.2.1 Direct FE-based Optimization

The optimization results obtained using the DGA - Ansys APDL framework demonstrate reliable for the 10-variable discrete design problem (Fig. 14). The best fitness value decreases steadily from the initial level of approximately 900 to a final value of $M_{best} \approx 627$ kg after 224 generations. The close agreement between the best and best-so-far curves indicates stable elitism and consistent improvement throughout the evolutionary process. The mean fitness evolution remains higher than the best fitness and exhibits pronounced oscillations, reflecting the strong nonlinearity of the structural response evaluated directly through finite element analysis. This behavior is typical for DGA implementations relying on high-fidelity solvers, where evaluation noise and constraint sensitivity are more pronounced. The population diversity remains relatively high and stable throughout the optimization process, indicating that the GA maintains sufficient exploration capability and avoids premature convergence. The gene evolution map shows gradual stabilization of several variables, while others continue to fluctuate until the final generations, suggesting complex interactions between discrete design variables and structural performance metrics.

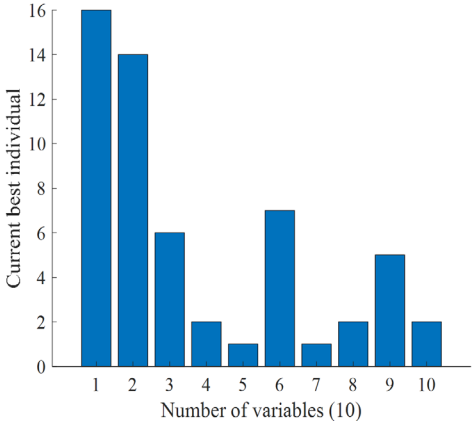

Fig. 15. Integer-coded design variables of the current best individual identified by the discrete GA– Ansys APDL optimization process

Figure 15 illustrates the configuration of the current best individual obtained from the optimization process, where the design variables are represented by integer indices corresponding to feasible configuration options. The results indicate that several variables tend to converge toward lower or boundary values, reflecting the tendency to reduce the frame mass while still satisfying the displacement and natural frequency constraints. In contrast, other variables remain at moderate or higher levels, highlighting their critical role in maintaining structural stiffness and dynamic stability. Overall, the obtained solution demonstrates that the discrete GA-Ansys APDL approach effectively achieves a balanced trade-off between frame mass minimization and structural performance requirements, thereby confirming the efficiency of the proposed optimization framework for the design of large-scale 3D concrete printer frames.

Notably, the total optimization time of approximately 38.5 hours (138,479.4 s) highlights the substantial computational cost associated with direct APDL-based finite element evaluations. While the GA-APDL approach provides high-fidelity and physically accurate results, the obtained solution is less optimal in terms of objective value and substantially more time-consuming.

The best solution corresponding to the minimum frame mass, while satisfying the displacement and natural frequency constraints, is represented by the normalized design vector: $\mathbf{x}_{best} = [0.6000, 0.5600, 0.0750, 0.0011, 0.0300, 0.0020, 0.0300, 0.0011, 0.0600, 0.0011]$.

3.2.2 ANN-based Surrogate Optimization

In Figure 16, the optimization results demonstrate that the proposed ANN-GA framework achieves stable and effective convergence for the mass minimization of a 3D concrete printer subject to displacement and first natural frequency constraints in Eq. (8). The best fitness value decreases rapidly during the early generations, from an initial level exceeding 900 to approximately 700 within the first 50 generations, and then gradually improves until reaching an optimal value of $M_{best} \approx 600$ kg at generation 219. The best and best-so-far curves nearly coincide, indicating that the algorithm has identified a high-quality solution region and successfully preserved elite individuals through the elitism strategy.

The mean fitness evolution fluctuates around $(6 \text{ to } 7) \times 10^3$, remaining significantly higher than the best fitness value. This behavior is typical for constrained and highly nonlinear optimization problems and indicates that population diversity is intentionally maintained to enhance global exploration. Such behavior confirms that the algorithm does not suffer from premature convergence. The population diversity, quantified by the standard deviation across all genes, exhibits a sharp reduction in the initial generations, followed by a relatively stable level ranging from approximately 3.6 to 4.2. This trend reflects a well-balanced trade-off between exploitation and exploration, which is particularly important for discrete combinatorial design spaces involving multiple variables. The heatmap of the best individual gene evolution reveals that several design variables converge rapidly to their optimal discrete indices, whereas others continue to evolve gradually over subsequent generations. This observation suggests differing sensitivities of the design variables with respect to the objective function and indicates that the final optimal configuration is both stable and physically meaningful. In terms of computational efficiency, the total optimization time of approximately 200 s for 219 generations with 10 design variables highlights the effectiveness of the surrogate ANN model in notably reducing the computational cost compared to direct finite element evaluations. Overall, the results confirm that the proposed ANN-GA framework provides a robust, efficient, and scalable solution for discrete structural optimization problems involving large-scale 3D printing systems with static and dynamic constraints. The best solution (Fig. 17) corresponding to the minimum frame mass is $\mathbf{x}_{best\_ANN} = [0.58, 0.58, 0.075, 0.001, 0.06, 0.001, 0.03, 0.001, 0.04, 0.0018]$.

The optimal design obtained using the ANN-GA approach was further verified using ANSYS software, as presented in Table 4 and Fig. 18. It can be observed that the discrepancies between the

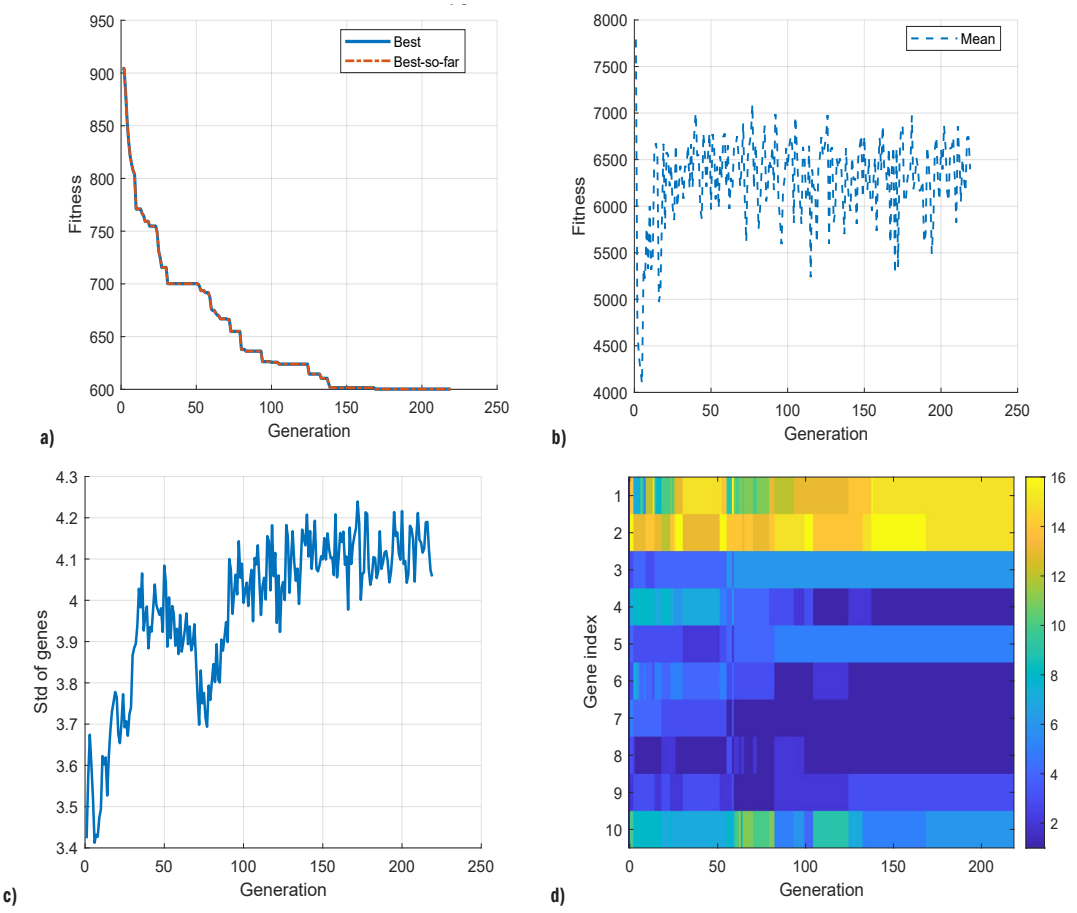

Fig. 16. Convergence characteristics of the discrete ANN-GA optimization for frame mass minimization; a) best and best-so-far fitness values, b) mean fitness value, c) population diversity, and d) evolution of the best individual

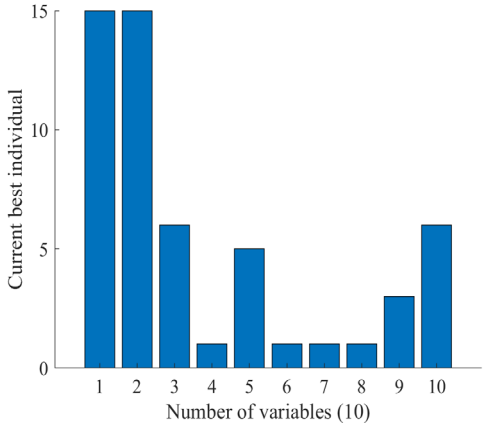

Fig. 17. Integer-coded design variables of the current best individual identified by the discrete ANN-GA optimization process

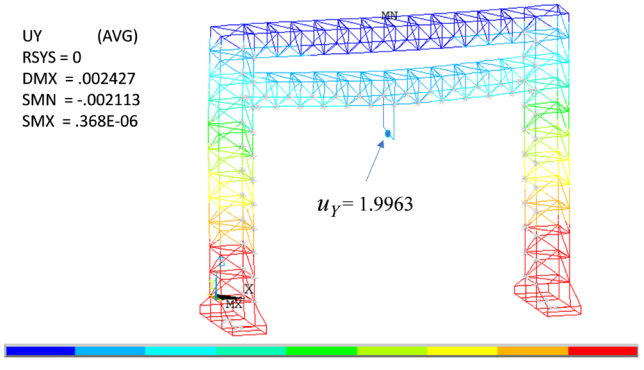

Fig. 18. Verification results (u_Y) of the ANN-GA optimal design in ANSYS®

Table 4. Verification of the GA-ANN optimal design using ANSYS®

Design option	u_X	u_Y	u_Z	f_1
GA-ANN	1.4393 mm	1.9987 mm	0.9898 mm	6.7287 Hz
APDL based	1.3718 mm	1.9963 mm	0.9927 mm	6.7152 Hz
Relative error	4.9 %	1.2 %	2.9 %	2.0 %

results predicted by the ANN surrogate model and those obtained from the ANSYS finite element simulations are relatively small, with deviations of less than 5 %.

The performance of the two optimization approaches is systematically compared in terms of both solution quality and computational efficiency.

3.3 Comparison and Discussion

In addition, the authors solved the APDL-GA optimization problem over a continuous design space. The resulting optimum provides a theoretically favorable set of parameters; however, it is difficult to implement in practice, since several optimal dimensions do not comply with the available standard hollow steel sections used in fabrication. The total optimization time was approximately 180,919 s,

highlighting the considerable computational cost of directly coupling GA with the finite element model. To improve manufacturability, the optimal continuous solution was subsequently mapped to a feasible design using a nearest-neighbor selection strategy, in which each continuous variable was adjusted to the closest admissible standard-section dimension while preserving proximity to the optimal solution. The final selected parameters are reported in Table 5.

Table 5 provides a comprehensive comparison between the experience-based selection (S-EXP) and various optimization strategies, including APDL-GA and ANN-GA approaches under both continuous and discrete design domains. Compared with the baseline S–EXP design (M = 974.5 kg), all optimization methods achieve a significant reduction in structural mass while satisfying displacement and dynamic constraints.

The APDL-GA optimization in the continuous domain reduces the mass by approximately 28 %, whereas the reselected-parameter variant further improves the reduction to about 35.7 %, indicating the sensitivity of the optimization outcome to parameter selection. A comparable mass reduction (35.6 %) is obtained using the APDL-GA approach in the discrete design domain, confirming that discretizing the design variables preserves the overall effectiveness of the optimization process.

Clearly, the ANN-GA method yields the best performance, achieving the maximum mass reduction of 38.4 % while maintaining displacement responses and first natural frequency values close to those obtained by Ansys APDL-based solutions. More importantly, the computational time is dramatically reduced from several tens of hours for GA-APDL to approximately 200 s for the ANN-GA approach. This significant reduction highlights the advantage of the surrogate-based optimization in efficiently exploring the discrete design space while preserving structural performance.

The convergence behavior of the design variables provides important insight into the underlying mechanical mechanisms governing the optimization results. As shown in Table 5, with particular focus on the optimal ANN-GA solution, the global geometric parameters of the frame (c_X, c_Y) tend to increase toward higher values compared to the experience-based design. This trend indicates that enlarging the overall frame dimensions significantly enhances the global bending stiffness, leading to a reduction in printhead displacements (Fig. 6, Fig. 8), which is consistent with classical structural mechanics principles. Similarly, the cross-sectional width of the primary load-bearing members (a_1) converges to its upper bound, confirming that increasing section width is an effective strategy for improving structural stiffness (Fig. 10) with a relatively moderate increase in mass. In contrast, the thickness parameters (t_1, t_2) and the dimensions of secondary bracing members (a_3, t_3) tend to converge toward lower values. This behavior suggests that these variables have a limited contribution to global stiffness while significantly affecting the overall mass, and are therefore minimized during the optimization process. The parameters associated with the base frame (a_4, t_4) do not exhibit a clear tendency toward boundary values, indicating their relatively minor influence on both the global bending stiffness and overall mass. In terms of dynamic performance, the first natural frequency (f_1) of the optimized designs shows a slight decrease compared to S–EXP solution but remains within the prescribed constraints. This reflects a rational trade-off between dynamic stiffness and mass reduction. These results confirm that the obtained optimal solutions are physically meaningful and governed by the fundamental balance between stiffness enhancement and mass minimization.

These results highlight the practical advantages of the proposed framework. In particular, the discrete design formulation ensures that all optimized solutions are directly manufacturable without post-processing. Furthermore, the ANN-GA approach significantly reduces computational time while maintaining prediction accuracy, making it highly suitable for large-scale engineering applications.

Overall, the results confirm that the integration of ANN surrogate models with GA optimization provides a robust and computationally efficient strategy for high-dimensional structural optimization, particularly for real-world systems involving discrete design constraints.

4 CONCLUSIONS

This study developed an integrated ANN-GA framework for the multi-parameter design optimization of a large-scale concrete 3D printer frame in a discrete design space consistent with practical manufacturing requirements. The proposed framework effectively combines high-fidelity finite element modeling, surrogate-based learning, and intelligent optimization to address the challenges associated with the design of complex large-scale machine structures.

First, a finite element model of the printer frame was established using APDL scripting, enabling automated evaluation of printhead displacements along the X, Y, and Z directions, as well as the natural frequencies of the frame. Based on the FE-generated dataset, an ANN surrogate model was constructed to predict printhead displacements and natural frequencies. With a network architecture of 10–32–10–4, the ANN model achieved high prediction accuracy, with deviations of less than 4 % compared to the FE results. Subsequently, a mathematical optimization model of the printer frame was formulated with ten design variables and four constraints, targeting minimum structural weight. Two optimization strategies were investigated: direct GA-based optimization coupled with APDL simulations and surrogate-based optimization using the ANN model. The developed GA optimization framework enables the identification of optimal design parameters in both continuous and discrete design domains.

Table 5. Comparison of structural performance and computational efficiency among different optimization approaches

Design option	Design parameters $[c_X, c_Y, a_1, t_1, a_2, t_2, a_3, t_3, a_4, t_4]$	u_X [mm]	u_Y [mm]	u_Z [mm]	f_1 [Hz]	M [kg]	Compare to S–EXP [%]	Time [s]
S-EXP (Experience-based selection)	[0.46, 0.46, 0.06, 0.003, 0.05, 0.0025, 0.025, 0.001, 0.06, 0.003]	1.1	1.9	0.99	7.01	974.5		
APDL-GA (continuous domain)	[0.5843, 0.5338, 0.0660, 0.0014, 0.0364, 0.0016, 0.0303, 0.0010, 0.0441, 0.0018]	1.2	2.0	1.0	6.73	633.7	27.98	180919
APDL-GA (continuous domain) - reselected parameter	[0.58, 0.54, 0.06, 0.0014, 0.038, 0.0016, 0.03, 0.001, 0.0500, 0.0018]	1.2	2.0	1.0	6.69	626.9	35.67	
APDL-GA (discrete domain)	[0.60, 0.56, 0.075, 0.0011, 0.03, 0.002, 0.03, 0.0011, 0.06, 0.0011]	1.2	2.0	0.998	6.76	627.4	35.62	138479
ANN-GA (discrete domain)	[0.58, 0.58, 0.075, 0.001, 0.06, 0.001, 0.03, 0.001, 0.04, 0.0018]	1.4	2.0	0.992	6.72	600.2	38.4	~200

All optimal solutions were subsequently verified using ANSYS software. Several important findings were obtained. Using the direct GA-APDL approach, continuous-domain optimization reduced the frame weight from 974.5 kg (experience-based design) to 633.7 kg, corresponding to a reduction of 27.98 %, with a total computational time of approximately 50.2 hours. When optimization was performed in the discrete design domain, the optimal frame weight was further reduced to 627.4 kg, achieving a 35.62 % reduction within 38.4 hours. Notably, the GA-ANN surrogate-based optimization identified an optimal frame weight of 600.2 kg, representing a 38.4 % reduction, with a total computational time of only 200 seconds.

The proposed framework integrates discrete design optimization with surrogate-based techniques and has been successfully applied to a real large-scale structural system. The results demonstrate both practical manufacturability and substantial improvements in computational efficiency. Moreover, the proposed ANN-GA-based framework provides a general and scalable solution for the design optimization of complex mechanical systems. It can be effectively extended to applications such as large-scale CNC machines, gantry-based manufacturing equipment, and construction robots, where discrete design constraints and high computational cost are critical challenges.

References

[1] Nguyen-Van, V., Panda, B., Zhang, G., Nguyen-Xuan, H., Tran, P. Automation in Construction digital design computing and modelling for 3-D concrete printing. *Autom Constr 123* 103529 (2021) **DOI:10.1016/j.autcon.2020.103529**.

[2] Paul, S.C., van Zijl, G.P.A.G., Tan, M.J., Gibson, I. A review of 3D concrete printing systems and materials properties: current status and future research prospects. *Rapid Prototyp J 24* 784-798 (2018) **DOI:10.1108/RPJ-09-2016-0154**.

[3] Ngo, T.D., Kashani, A., Imbalzano, G., Nguyen, K.T.Q., Hui, D. Additive manufacturing (3D printing): A review of materials, methods, applications and challenges. *Compos Part B Eng 143* 172-196 (2018) **DOI:10.1016/j.compositesb.2018.02.012**.

[4] Záda, V., Belda, K. Structure Design and solution of kinematics of robot manipulator for 3D concrete printing. *IEEE Trans Autom Sci Eng 19* 3723-3734 (2022) **DOI:10.1109/TASE.2021.3133138**.

[5] Sahai, R., Bisht, R.S., Singh, S., Panigrahi, S.K. Design analysis and development of a gantry robot for multi-layer 3-D concrete printing with simulation and experimental validation. *Mech Based Des Struct Mach 53* 1001-1030 (2025) **DOI:10.1080/15397734.2024.2377266**.

[6] Jo, J.H., Jo, B.W., Cho, W., Kim, J.-H. Development of a 3D printer for concrete structures: Laboratory testing of cementitious materials. *Int J Concr Struct Mater 14* 13 (2020) **DOI:10.1186/s40069-019-0388-2**.

[7] Liu, S., Du, Y., Lin, M. Study on lightweight structural optimization design system for gantry machine tool. *Concurr Eng Res Appl 27* 170-185 (2019) **DOI:10.1177/1063293X19832940**.

[8] Zhao, L., Ma, J., Chen, W., Guo, H. Lightweight design and verification of gantry machining center crossbeam based on structural bionics. *J Bionic Eng 8* 201-206 (2011) **DOI:10.1016/S1672-6529(11)60021-8**.

[9] Kilavuz, F., Kıral, F.G. Design optimization of mechanical valves in dishwashers based on the minimization of pressure losses. *Stroj Vestn-J Mech E 70* 194-208 (2024) **DOI:10.5545/sv-jme.2023.768**.

[10] Li, H.F., Luo, M., Xu, T.T., Li, Q.Z., Hou, Z.M. Optimization method of multi-parameter coupling for a hydraulic rolling reshaper based on factorial design. *Stroj Vestn-J Mech E 69* 483-496 (2023) **DOI:10.5545/sv-jme.2023.627**.

[11] Ding, F., Lyu, H., Chen, J., Cao, H., Zhang, L. Multi-objective optimization design of the ejector plate for rear-loader garbage trucks. *Stroj Vestn-J Mech E 71* 169-178 (2025) **DOI:10.5545/sv-jme.2024.1185**.

[12] Du, D., Li, Y., Song, J., He, Z., Xu, J. Two-Stage optimal design of metro underframe structures: Based on topology-size-shape co-optimization methodology. *Stroj Vestn-J Mech E 71* 381-388 (2025) **DOI:10.5545/sv-jme.2025.1308**.

[13] Runge, G., Peters, J., Raatz, A. Design Optimization of soft pneumatic actuators using genetic algorithms. *IEEE Int Conf Robot Biomimetics* (2017) **DOI:10.1109/ROBIO.2017.8324449**.

[14] Tran, V.-L., Kim, S.-E. A practical ANN model for predicting the PSS of two-way reinforced concrete slabs. *Eng Comput 37* 2303-2327 (2020) **DOI:10.1007/s00366-020-00944-w**.

[15] Vu, Q.V., Tangaramvong, S., Van, T.H., Papazafeiropoulos, G. Hybrid GA-ANN and PSO-ANN methods for accurate prediction of uniaxial compression capacity of CFDST columns. *Steel Compos Struct 6* 759-779 (2023) **DOI:10.12989/scs.2023.47.6.759**.

[16] Papazafeiropoulos, G., Vu, Q.-V., Truong, V.-H., Luong, M.-C., Pham, V.-T. Prediction of buckling coefficient of stiffened plate girders using deep learning algorithm. *Lect Notes Civ Eng 54* 1143-1148 (2020) **DOI:10.1007/978-981-15-0802-8_183**.

[17] Wu, R.-T., Jahanshahi, M.R. Deep Convolutional Neural network for structural dynamic response estimation and system identification. *J Eng Mech* 1451 (2019) **DOI:10.1061/(asce)em.1943-7889.0001556**.

[18] Ye, Y., Scharff, R.B.N., Long, S., Han, C., Du, D. Modelling of soft fiber-reinforced bending actuators through transfer learning from a machine learning algorithm trained from FEM data. *Sens Actuators A Phys 368* 115095 (2024) **DOI:10.1016/j.sna.2024.115095**.

[19] Bührer Santana, P., Martins Gomes, H., Mendes Ferreira, A., Tita, V. A Multiobjective optimization framework for strength and stress concentration in variable axial composite shells: A metaheuristic approach. *Lat Am J Solids Struct 20* 1-16 (2022) **DOI:10.1590/1679-78257577**.

[20] Guo, Q., Wang, S. Free vibration analysis and optimal design of adhesively bonded double-strap joints by using artificial neural networks. *Lat Am J Solids Struct 17* 1-19 (2019) **DOI:10.1590/1679-78255878**.

[21] Jiang, H., Gao, L. Optimizing the rail profile for high-speed railways based on artificial neural network and genetic algorithm coupled method. *Sustainability 12* 658 (2020) **DOI:10.3390/su12020658**.

[22] Liu, X. Qin, J., Zhao, K., Featherston, C.A., Kennedy, D., Jing, Y., et al. Design optimization of laminated composite structures using artificial neural network and genetic algorithm. *Compos Struct 305* 116500 (2023) **DOI:10.1016/j.compstruct.2022.116500**.

[23] Zhang, X. Design optimization of irregularity RC structure based on ANN-PSO. *Heliyon 10* e27179 (2024) **DOI:10.1016/j.heliyon.2024.e27179**.

[24] Soori, M., Karimi, F., Jough, G. Artificial Intelligent in optimization of steel moment frame structures: A review. *Int J Struct Constr Eng 18* (2024) from *https://hal.science/hal-04525909*, accessed on 2026-02-02.

[25] Rosel Solís, M., Dávalos Ramírez, J., Molina Salazar, J., Ruiz Ochoa, J., & Gómez Roa, A. Optimization of running blade prosthetics utilizing crow search algorithm assisted by artificial neural networks. *Stroj Vestn-J Mech E 67* 88-100 (2021) **DOI:10.5545/sv-jme.2020.6990**.

[26] Dávalos, O., Caldiño-Herrera, U., Cornejo-Monroy, D., Tenango-Pirin, O., Garcia, J., & Basurto-Pensado, M. Reduction of stresses and mass of an engine rubber mount subject to mechanical vibrations. *Stroj Vestn-J Mech E 67* 101-113 (2021) **DOI:10.5545/sv-jme.2020.7051**.

[27] Binh, P.V., Binh, H.P., Hai, T.D., Tung, P.Đ. Mechanical design and structural optimization of the frame of a large-scale gantry 3D concrete printer. *J Sci Tech 18* 38-54 (2023) **DOI:10.56651/lqdtu.jst.v18.n01.582**.

[28] Bathe, K.J. *Finite Element Procedures,* Prentice-Hall, Hoboken (2005).

[29] Clough, R.W. *Dynamics of Structures, 3rd ed.* CRC Press, London (1995) **DOI:10.1201/b11772**.

[30] Rezapourian, M., Darabi, A.C., Khoshbin, M., Schmauder, S., Hussainova, I. Surrogate-model prediction of mechanical response in architected Ti6Al4V cylindrical TPMS metamaterials. *Metals 15* 1372 (2025) **DOI:10.3390/met15121372**.

[31] Marković, E., Marohnić, T., Basan, R. A surrogate artificial neural network model for estimating the fatigue life of steel components based on finite element simulations. *Materials* (2025) **DOI:10.3390/ma18122756**.

[32] Zain, A.M., Haron, H., Sharif, S. Prediction of surface roughness in the end milling machining using artificial neural network. *Expert Syst Appl 37* 1755-1768 (2010) **DOI:10.1016/j.eswa.2009.07.033**.

[33] Dang, H.M., Bui, V.P., Phung, V.B., Thom, D.V., Minh, P.V., Gavriushin, S.S. et al. Development of generalized mathematical model for slider-crank mechanism synthesis based on approach of multiobjective concurrent engineering and application. *Arab J Sci Eng 46* 8037-8053 (2021) **DOI:10.1007/s13369-021-05627-2**.

[34] Ji, Q., Li, C., Zhu, D., Jin, Y., Lv, Y., He, J. Structural design optimization of moving component in CNC machine tool for energy saving. *J Clean Prod 246* 1188976 (2019) **DOI:10.1016/j.jclepro.2019.118976**.

Acknowledgements *This research was supported by the Program "Supporting Research, Development and Technology Application of Industry 4.0" (KC-4.0/19-25) of the Ministry of Science and Technology in Vietnam through the funding of the Project "Research, Design, and Manufacturing*

of a Large-Scale Concrete 3D Printing System Applied in the Construction Industry", no. KC-4.0-36/19-25.

Received *2026-02-02,* **revised** *2026-05-06,* **accepted** *2026-05-22 as Original Scientific paper.*

Data Availability *The data that support the findings of this study are available from the corresponding author upon reasonable request.*

Author Contribution *Duc Hai Ta: Data curation, Resources, Writing-original draft; Dinh Tung Pham: Funding acquisition, Project administration; Van Binh Phung: Writing-original draft; Writing-review & editing, Conceptualization, Methodology.*

Integriran pristop na osnovi ANN–GA za večparametrično optimizacijo oblike ogrodja velikega 3D-tiskalnika za beton v diskretnem optimizacijskem prostoru

Povzetek *V članku je predstavljen integriran pristop za večparametrično optimizacijo oblike ogrodja velikega 3D-tiskalnika za beton, ki temelji na kombinaciji umetnih nevronskih mrež in genetskih algoritmov (ANN–GA). Na podlagi praktičnih konstrukcijskih zahtev in obratovalnih pogojev je bil z uporabo skriptnega jezika APDL® razvit model ogrodja tiskalnika z metodo končnih elementov (MKE), ki omogoča avtomatizirano vrednotenje odklona tiskalne glave in lastnih frekvenc konstrukcije. Na osnovi podatkov, pridobljenih z analizami MKE, je bila naučena večplastna usmerjena nevronska mreža (MLFFNN), uporabljena kot nadomestni model za napovedovanje strukturnih odzivov ogrodja. Parametrične raziskave so pokazale, da nadomestni model na osnovi nevronske mreže bistveno zmanjša računski čas ob hkratnem ohranjanju visoke natančnosti napovedi, saj se napake v primerjavi z neposredno analizo MKE gibljejo med 1 % in 4 %. Nato je bil oblikovan optimizacijski model za minimizacijo mase z desetimi projektnimi spremenljivkami in štirimi omejitvami, povezanimi z odklonom tiskalne glave in lastnimi frekvencami. Za reševanje optimizacijskega problema so bili uporabljeni genetski algoritmi na dva načina: neposredna optimizacija, povezana z analizo MKE, in optimizacija z uporabo nadomestnega modela ANN. Posebnost raziskave je, da je bila optimizacija izvedena v diskretnem optimizacijskem prostoru, skladnim s standardnimi dimenzijami komercialno dostopnih jeklenih votlih profilov. Rešitve, pridobljene z različnimi optimizacijskimi strategijami, vključno z zveznimi in diskretnimi modeli MKE, nadomestnim modelom ANN ter obliko na podlagi inženirskih izkušenj, so bile sistematično primerjane. Rezultati kažejo, da predlagan pristop omogoča zmanjšanje mase konstrukcije za 27 % do 38 % v primerjavi z začetno obliko, ki temelji samo na izkušnjah. Poleg tega optimizacija z uporabo nadomestnega modela ANN skrajša skupni računski čas s približno 38 ur na približno 200 sekund, kar jasno dokazuje učinkovitost in praktično uporabnost predlaganega pristopa za načrtovanje velikih industrijskih strojev.*

Ključne besede *ogrodje 3D-tiskalnika za beton, optimizacija oblike, nadomestni model ANN, integriran pristop ANN–GA*